# Radiometric compensation algorithm for color reproduction of projection display on patterned surface

**Wenhai Zou (邹文海), Haisong Xu (徐海松)*, and Weige Lü (吕玮阁)**

*State Key Laboratory of Modern Optical Instrumentation, Zhejiang University, Hangzhou 310027, China*

**E-mail: chsxu@zju.edu.cn*

Received August 19, 2009

A novel radiometric compensation algorithm is proposed to correct the color distortions of the projection display on patterned surface. Two choices of the objective image are investigated in this algorithm. A linear compression followed by a sigmoid-function transformation based on the statistical parameters of the compensating radiance map is performed to reduce the clippings of the compensating color and expected to properly reproduce the dynamic range and the visibility of the image content. Three types of projection displays are produced for each test image. The parameter analysis indicates that the compensated displays could well conceal the surface pattern and tend to exhibit higher lightness or lightness contrast in the camera. The comparison results in a psychophysical experiment demonstrate that all the compensated displays outperform the uncompensated ones. The original input images seem more appropriate to be selected as the objective images, and the predicted objectives on the white screen are just proper for the bright and low-contrast input images displayed on the faint surface.

*OCIS codes:* 120.2040, 330.1715, 100.200, 100.5010.

*doi: 10.3788/COL20100804.0388.*

A novel type of projection displays has been evolving in the past few years. This type of displays does not restrictively work on the perfect white screen but onto the other patterned surfaces, such as colored doors, brick walls, paintings, textured boxes, etc. Owing to the varying reflectance of these surfaces resulting in the color imperfections for the display images, the projector-camera (ProCam) systems by attaching an environment-sensing camera into the traditional projector have been used to characterize the color transformations of the display[1,2] in advance and then compensate them via a specified algorithm. To date, many efforts have been done to enhance the characterization and compensation of the projection displays on the patterned surface. Nayar *et al.* used a 3×3 matrix and several images to characterize the surface reflectance together with the color mixing of the ProCam system for each pixel and compensated the surface imperfections online by inversing these metrics onto the input image[3−5]. What is more, in order to achieve real-time compensation for multi-projector systems, Bimber *et al.* simplified the display characterization using a reflectance factor and scaled the input color value for each channel to obtain the compensating image[6]. In these works, the input image is directly adopted as the objective image, which, whereas, usually causes clippings in the compensated output because of the limited dynamic range of the projector. Thereafter, Ashdown *et al.* firstly pre-calibrated the ProCam system offline and predicted the display image on the perfect white screen under ideal conditions, which was adopted as the compensation objective[7]. In this method, the objective image is cautiously revised to reduce the color deficiencies of the display image, however, the high time cost makes it restrictedly suitable to static environment. More recently, Son *et al.* pre-captured the white images projected on the white screen and the patterned surface respectively, and obtained the compensated image by using a luminance compensation followed by a chromaticity correction[8]. In our previous work[9], the ProCam system was characterized by using a polynomial model, and then the surface parameters were recovered efficiently to form the compensation algorithm. The efficiencies are highly improved by simple operations in these approaches, but the adaptive range of the surface reflectance is greatly undermined at the same time. In this letter, a novel compensation algorithm is further developed to improve the flexibility of the ProCam system.

For the projection display on the patterned surface based on the ProCam system, a radiometric model can be established to describe its data flow of the image. The digital values $\mathbf{I}_{\rm in} = [r_{\rm in},\ g_{\rm in},\ b_{\rm in}]^{\rm T}$ of the color for each pixel $(x,\ y)$ in the input image is processed by the projector of the system and transformed to the projected radiance $\mathbf{P} = [p_{\rm r},\ p_{\rm g},\ p_{\rm b}]^{\rm T}$ as

$$\mathbf{P} = f_{\rm p}\left(\mathbf{I}_{\rm in}\right), \tag{1}$$

where $f_{\rm p}$ represents the spatially invariant transmission function of the projector. We note that the mixing[3] between the projector and the camera is also involved into $f_{\rm p}$. The projected radiance together with the irradiance $\mathbf{E} = [e_{\rm r},\ e_{\rm g},\ e_{\rm b}]^{\rm T}$ of the environmental lighting is modulated by the surface reflectance and finally reaches the camera. Assuming that the reflectance of the surface is independent within each of the camera channel[5], this procedure can be modelled as

$$\mathbf{C} = \mathbf{K}\left(\mathbf{P} + \mathbf{E}\right), \tag{2}$$

where $\mathbf{C} = [c_{\rm r},\ c_{\rm g},\ c_{\rm b}]^{\rm T}$ is the irradiance of the captured image for the camera, and $\mathbf{K} = {\rm diag}(k_{\rm r},\ k_{\rm g},\ k_{\rm b})$ is the surface reflectance matrix. The captured irradiance is converted and mapped to the digital values $\mathbf{I}_{\rm out} = [r_{\rm out},\ g_{\rm out},\ b_{\rm out}]^{\rm T}$ of the color in the output image at the corresponding pixel $(u,\ v)$ of the camera as

$$\mathbf{I}_{\rm out} = f_{\rm c}\left(\mathbf{C}\right), \tag{3}$$

 

where $f_c$ represents the spatially invariant response function of the camera. The correspondence between $(x, y)$ and $(u, v)$ can be constructed and stored as a look-up table by means of a geometric calibration operation[3], and all of the parameters $f_c$, $\mathbf{K}$, $\mathbf{E}$, $f_p$ can be acquired via a characterization procedure in advance. $f_c$ can be efficiently measured independent of any aid of the device or material using multi-exposure technique[10]. The white image projected onto the perfect white screen by the projector is memorized as the white reference for the camera of the ProCam system. $\mathbf{K}$ and $\mathbf{E}$ can be directly obtained by projecting and capturing a black and a white images on the patterned surface respectively, and $f_p$ can be recovered using a group of gray images and a patch image based on our previous work[11]. In this study, $f_c$ and $f_p$ are stored as two groups of three one-dimensional (3-1D) look up tables, while $\mathbf{K}$ and $\mathbf{E}$ are obtained as two images.

The compensating image can be calculated within four steps as follows. Firstly, the objective image should be determined according to the content of the input image. Although reproducing the visual appearance of the input image is the ultimate goal of the compensation, defining and quantifying the visual appearance is a difficult issue and still being explored presently. Taking the camera of the ProCam system as the proxy of the viewer, the objective images are equivalent to the output images, and two general approaches for their determination are tentatively investigated. On one hand, the color for each pixel $(x, y)$ in the input image is directly selected to be that of the corresponding pixel $(u, v)$ in the objective image as

$$\mathbf{I}_{\rm obj} = \mathbf{I}_{\rm in}, \tag{4}$$

for the accurate reproduction of the input image in the camera. On the other hand, if the objective image is expected to be exactly the same as that on the perfect white screen without environmental lighting, the color for each pixel $(u, v)$ in the objective image can be predicted as

$$\mathbf{I}_{\rm obj} = f_c\left[f_p\left(\mathbf{I}_{\rm in}\right)\right], \tag{5}$$

supposing that the reflectance factor of the perfect white screen is diag(1, 1, 1).

Secondly, the compensating radiance $\mathbf{P}_{\rm pc} = [p^{\rm r}_{\rm pc}, p^{\rm g}_{\rm pc}, p^{\rm b}_{\rm pc}]^{\rm T}$ can be pre-calculated from the objective color as

$$\mathbf{P}_{\rm pc} = \mathbf{K}^{-1}\left[f_c^{-1}\left(\mathbf{I}_{\rm obj}\right) - \mathbf{K}\mathbf{E}\right], \tag{6}$$

where $f_c^{-1}$ represents the reverse of $f_c$. However, due to the limited dynamic range of the existing projector, the compensating radiance is usually out of the capability of the ProCam system especially for the sharp edge in the surface pattern, which would result in clippings in the compensating color.

Thirdly, the compensating radiance should be further mapped to the available dynamic range of the projector output to avoid the clipping error. Based on the fact that the rod photoreceptor of human visual system will lose the sensitivity to any additional light intensity when adapted to a dark scene[12], this mapping is carried out in the form of a sigmoid function for each color channel independently. The minimal dynamic range $[\delta, \beta]$ for all the three color channels, R, G, and B, of the projector output is determined using $f_p$ beforehand, and the minimal, mean, and maximum values for all the three channels of the compensating radiance map (CRM) after ignoring the brightest and dimmest 0.1% pixels are then estimated, respectively. Thereafter, the transformed compensating radiance $\mathbf{P}_{\rm tc} = [p^{\rm r}_{\rm tc}, p^{\rm g}_{\rm tc}, p^{\rm b}_{\rm tc}]^{\rm T}$ is expressed as

$$\boldsymbol{p}^{\rm i}_{\rm tc} = \begin{cases} \delta + (m-\delta)\left(\frac{x_{\rm i}-\delta}{m-\delta}\right)^2, & \delta \le x_{\rm i} \le m \\ \beta - (\beta - m)\left(\frac{\beta - x_{\rm i}}{\beta - m}\right)^2, & m \le x_{\rm i} \le \beta \end{cases}, \tag{7}$$

where

$$x_{\rm i} = (\beta - \delta)\left(p^{\rm i}_{\rm pc} - {\rm Min}\right)({\rm Max} - {\rm Min})^{-1} + \delta,$$
$$m = (\beta - \delta)\left({\rm Mean} - {\rm Min}\right)({\rm Max} - {\rm Min})^{-1} + \delta,$$
$${\rm i} = {\rm r},\ {\rm g},\ {\rm b}.$$

We note that the ratios among the components of the compensating radiance keep constant during the mapping, and this is crucial for the compensation of the surface color according to the radiometric model. Moreover, if the range [Min, Max] of the CRM is larger than the range $[\delta, \beta]$, the dynamic range of the CRM will be compressed. Contrarily, the dynamic range will be stretched. In addition, as shown in Fig. 1, the shape of the sigmoid function will be sensitively adjusted with the variation of the parameter $m$ to keep the visibility for the central part of the content in the CRM, and with the increasing $m$, the dynamic range of the CRM will be compressed in the lower section but expanded in the higher section.

Finally, the compensating color $\mathbf{I}_{\rm cmp}$ for the patterned surface display can be expressed as

$$\mathbf{I}_{\rm cmp} = f_p^{-1}\left(\mathbf{P}_{\rm tc}\right), \tag{8}$$

where $f_p^{-1}$ represents the reverse of $f_p$. Experiments were accomplished for this developed algorithm, and a VGA NEC LT 30+ projector with a native resolution of 1024 × 768 pixels and a HITACHI HV-D30 camera with a resolution of 768 × 576 pixels were used to set up the ProCam system. The images were projected onto the screen via a RADEON R9200SE display card, and those images from the camera were captured by an 8-bit Matrox Meteor II/Multi-channel frame-grabber. Several patterned posters were prepared to serve as the test surfaces and two of them, designated as "Patch" and "Flower", are illustrated in Fig. 2. A group of ISO standard digital images are selected as the test images, and two examples of them are given as Nos. 1 and 2 in

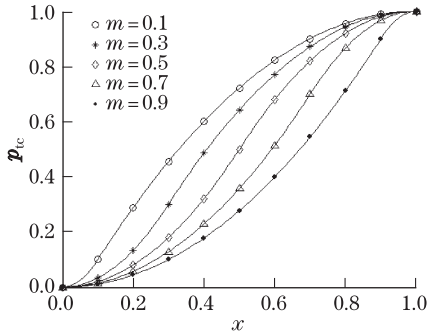


Fig. 1. Shape of the sigmoid function changes with the parameter $m$.

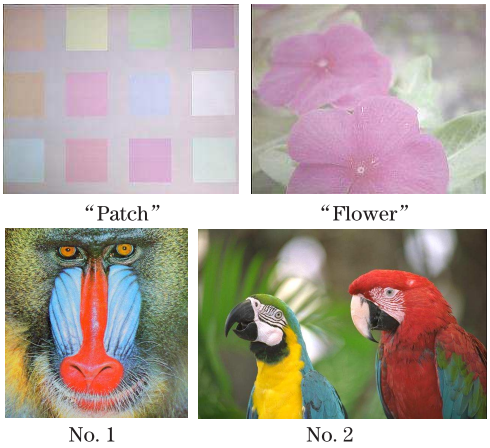


Fig. 2. Examples of test surfaces ("Patch" and "Flower") and test images (Nos. 1 and 2).

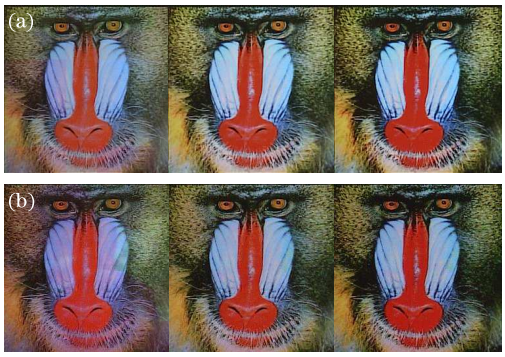


Fig. 3. UD (left), $CD_{do}$ (middle), and $CD_{po}$ (right) for No. 1 test image on the different surfaces. (a) On "Patch" surface; (b) on "Flower" surface.

Fig. 2. For each test image, three projection displays, including the uncompensated display (UD) and two types of compensated displays (CDs) for different compensating objectives ($CD_{do}$ for the input image directly as the objective and $CD_{po}$ for the predicted image on the white screen as the objective), were produced on each test surface. As shown in Figs. 3 and 4, three displays for the Nos. 1 and 2 images on each surface were captured with the camera of the ProCam system to exhibit the difference between them.


Fig. 4. UD (left), $CD_{do}$ (middle), and $CD_{po}$ (right) for No. 2 test image on the different surfaces. (a) On "Patch" surface; (b) on "Flower" surface.

By comparing the output images in pairs, it could be seen that the pattern of the surfaces could be distinctly discriminated from the image content in the UD, while hardly identified in the CDs, which was relatively more obvious on the "Flower" surface. Furthermore, the image lightness $L_Y$ and the lightness contrast $T_Y$, were calculated to reveal the visibility of these output images, as listed in Table 1. $L_Y$ and $T_Y$ are expressed as

$$L_Y = \frac{1}{N}\sum_{i=1}^{N} Y_i,$$
$$T_Y = \frac{\max(Y_i) - L_Y}{L_Y}, i = 1, 2, \cdots, N, \tag{9}$$

where $N$ is the number of the compared pixels, and $\max(\cdot)$ is used to find the maximum of all the pixel values in the image. The $Y$ values are calculated as

$$Y = 0.299 r_{\text{out}} + 0.587 g_{\text{out}} + 0.114 b_{\text{out}}. \tag{10}$$

As seen from the data in Table 1, $CD_{do}$ seems to be brighter than $CD_{po}$, and $CD_{po}$ presents the highest lightness contrast whilst the lowest lightness for different test images on each surface.

In order to evaluate the total appearance of each display, the three displays for each test image were also visually compared by a panel of 15 observers using the psychophysical method of rank order for their preference choices on each test surface. The visual experiments were directly carried out on the test surfaces under the dim office lighting environment. The ProCam system and the subjects were about 1.6 and 3.0 m away, respectively,

**Table 1. Parameters of the Captured Displays for the Two Test Images on Different Surfaces with $[\delta, \beta] = [0.004, 0.992]$**

| Test Surface | Test Images | | Min | Max | Mean | $m$ | $L_Y$ | $T_Y$ |
|---|---|---|---|---|---|---|---|---|
| "Patch" | No. 1 | UD | – | – | – | – | 98.49 | 0.8501 |
| | | $CD_{do}$ | 0 | 1.365 | 0.435 | 0.318 | 105.99 | 0.9629 |
| | | $CD_{po}$ | 0 | 1.318 | 0.388 | 0.294 | 94.51 | 1.2033 |
| | No. 2 | UD | – | – | – | – | 77.14 | 1.7779 |
| | | $CD_{do}$ | 0 | 1.824 | 0.333 | 0.182 | 77.27 | 1.7468 |
| | | $CD_{po}$ | 0 | 1.831 | 0.340 | 0.186 | 64.71 | 2.2802 |
| "Flower" | No. 1 | UD | – | – | – | – | 89.59 | 1.1069 |
| | | $CD_{do}$ | 0.004 | 2.055 | 0.563 | 0.272 | 91.41 | 0.9288 |
| | | $CD_{po}$ | 0 | 2.016 | 0.502 | 0.249 | 81.45 | 1.1762 |
| | No. 2 | UD | – | – | – | – | 68.59 | 2.0823 |
| | | $CD_{do}$ | 0.004 | 2.820 | 0.445 | 0.157 | 65.74 | 1.8172 |
| | | $CD_{po}$ | 0 | 2.937 | 0.446 | 0.152 | 54.71 | 2.3614 |

**Table 2. Ranked Frequencies and $z$-Scores for Each Display in the Psychophysical Experiment on Different Test Surfaces**

| Test Images | | "Patch" Surface | | | | "Flower" Surface | | | |
|---|---|---|---|---|---|---|---|---|---|
| | | Ranked Frequency | | | $z$-Score | Ranked Frequency | | | $z$-Score |
| | | 1st | 2nd | 3rd | | 1st | 2nd | 3rd | |
| No. 1 | UD | 4 | 2 | 9 | −0.430 | 1 | 1 | 13 | −1.306 |
| | $CD_{do}$ | 6 | 7 | 2 | 0.342 | 9 | 6 | 0 | 0.966 |
| | $CD_{po}$ | 5 | 6 | 4 | 0.088 | 5 | 8 | 2 | 0.340 |
| No. 2 | UD | 2 | 5 | 8 | −0.597 | 1 | 4 | 10 | −0.966 |
| | $CD_{do}$ | 12 | 2 | 1 | 1.110 | 10 | 5 | 0 | 1.062 |
| | $CD_{po}$ | 1 | 8 | 6 | −0.513 | 4 | 6 | 5 | −0.096 |

from the test surfaces. The three displays for each test image were randomly presented and ranked by individual observers according to their preference degree from most (1st), second (2nd) to least (3rd) preferred choices and the assessment time was not restrained. As listed in Table 2, the frequencies of each degree for every image were counted and transformed to $z$-score, which is a measure of the distance of a score from the mean of a distribution in standard deviation units[13], and a higher $z$-score represented a greater preference degree in this study.

From the $z$-scores of the three displays, it could be seen that the preference orders were almost the same for the different test images on individual surfaces. $CD_{do}$ was the first-rate, followed by $CD_{po}$, and UD was in the third place. For the image No. 1, both the two CDs obviously outperformed UD, while $CD_{do}$ was prior to $CD_{po}$ on each surface. The same phenomenon could be found for the image No. 2 on the "Flower" surface. However, for the image No. 2 on the "Patch" surface, $CD_{do}$ clearly surpassed UD, but there was no significant difference between $CD_{po}$ and UD. The experimental results indicate that the proposed algorithm could effectively compensate the influences of the surface imperfections for the patterned surface projection displays, and the original input image rather than its predicted output image on the perfect white screen is preferred to be adopted as the objective image for this algorithm. In addition, the compensated displays of the predicted objectives would be produced with the higher lightness contrast but the lower lightness, which implies that the predicted objectives in the proposed algorithm are only favorable for the low-contrast and bright images projected upon the less reflected surface.

In conclusion, a radiometric compensation algorithm is proposed to enable the projection display on the patterned surface. Two general purposes for the determination of objective image are discussed. A sigmoid function is introduced to reduce the clippings of the compensating image and keep proper reproduction of the lightness contrast of the image. Meanwhile, due to the shape of the sigmoid function being sewed according to the statistical characteristics of the compensating radiance map, the lightness of the compensated display could be well reserved and even be enhanced. For each test image, an uncompensated display and two compensated displays could be produced on the test surfaces. To reveal the difference among three displays, a camera-vision-based comparison and a visual experiment are performed respectively. The evaluation results indicate that the compensated displays could well repair the imperfections of the surfaces and be presented with the higher lightness or lightness contrast. The statistical data of the visual assessment also verify that the quality of the compensated display outperforms the uncompensated one. The compensated displays by adopting the original input image as the objective image are most preferred by the observers for different test images while the predicted images on the perfect white screen as the objective images are only appreciated for the bright and low-contrast input images on the low-reflectance surface. Because of the complex computation process being not included in the calculation of the compensating color, the proposed algorithm is beneficial for the dynamic adaptation. However, the chroma distortion of the compensating color is not accurately controlled in its computation, so this algorithm is principally adaptive to the unsaturated color surface.

## References


1. W. Yang, N. Liao, Q. Huang, J. Hao, and S. Jiang, Acta Opt. Sin. (in Chinese) **24,** 1039 (2004).
2. X. Zhang and H. Xu, Acta Opt. Sin. (in Chinese) **27,** 1719 (2007).
3. S. K. Nayar, H. Peri, M. D. Grossberg, and P. N. Belhumeur, in *Proceedings of IEEE Workshop on Projector Camera Systems* (2003).
4. M. D. Grossberg, H. Peri, S. K. Nayar, and P. N. Belhumeur, in *Proceedings of IEEE Conference on CVPR* 452 (2004).
5. K. Fujii, M. D. Grossberg, and S. K. Nayar, in *Proceedings of IEEE Computer Society Conference on CVPR* 814 (2005).
6. O. Bimber, A. Emmerling, and T. Klemmer, Computer **38,** 48 (2005).
7. M. Ashdown, T. Okabe, I. Sato, and Y. Sato, in *Proceedings of IEEE Computer Society Conference on CVPR* 6 (2006).
8. C.-H. Son and Y.-H. Ha, J. Imag. Sci. Technol. **52,** 1 (2008).
9. W. Zou , H. Xu , B. Han, and D. Park, Chin. Opt. Lett. **6,** 499 (2008).
10. P. E. Debevec and J. Malik, in *Proceedings of ACM SIGGRAPH* 369 (1997).
11. W. Zou and H. Xu, Chin. Opt. Lett. **7,** 479 (2009).
12. E. H. Adelson, Vision Res. **22,** 1299 (1982).
13. W. H. Ehrenstein and A. Ehrenstein, in U. Windhorst and H. Johansson, (eds.) *Modern Technique in Neuroscience Reasearch* (Springer, Berlin, 1999) chap. 43.